ELSEVIER

Chemical Physics 232 (1998) 353–360

Chemical Physics

Marta Castillejo [a], Stelios Couris [b], Eoin Lane [b], Margarita Martin [a,*], Javier Ruiz [c]

[a] *Instituto de Química Física ''Rocasolano'', C.S.I.C. Serrano 119, 28006 Madrid, Spain*

[b] *I.E.S.L.–FORTH, P.O. Box 1527, Heraklion 711 10, Crete, Greece*

[c] *Departamento de Física Aplicada, Facultad de Ciencias, Universidad de Málaga, Campus de Teatinos, Málaga, Spain*

Received 7 January 1998

Abstract

Ketene in a molecular beam is excited at the onset of its $\tilde{X}\,^1A_1 \rightarrow \tilde{B}\,^1B_1$ absorption band by laser light at 230 nm. The rovibrational population distribution in the CO photofragment, formed in the dissociation, is probed by REMPI. The phase space theory (PST) is applied to the dissociation channels leading respectively to $CO + CH_2(\tilde{a}\,^1A_1)$ and $CO + CH_2(\tilde{b}\,^1B_1)$. For the latter, the PST calculations lead to an average rotational energy in CO which is not compatible with the measured value, thus suggesting that this channel does not represent an important contribution to the dissociation process.

1. Introduction

The dissociation dynamics of ketene, excited at energies from 200 to 2900 cm^{-1} above the first singlet dissociation threshold, has been studied in great detail [1–6]; dissociation rates [7] and relative yields of singlet vs. triplet channels have been measured, as a function of the excess energy above the dissociation threshold [8,9]. Much less work has been focused on the high-lying $\tilde{B}\,^1B_1$ state of ketene [10,11]. The onset of the band absorption starts at $\lambda \approx 230$ nm; the band shows some broad features attributed to vibrational structure [12]. Several dissociation channels are energetically accessible: the most exoergic is the spin-forbidden process leading to ground-state CO and $\tilde{X}\,^3B_1$; the singlet dissociation channel opens at energies above 30116 cm^{-1}, being more exothermal than the triplet channel by 3156 cm^{-1}; the next singlet channel forming $CH_2(\tilde{b}\,^1B_1)$ is less exoergic than the triplet channel by 11539 cm^{-1}; C–H bond cleavage requires ~ 3000 cm^{-1} less energy than the latter. Little is known about the branching ratio and dependence on excitation energy of the different dissociation pathways. The exit channel forming methylene in the $\tilde{b}\,^1B_1$ state has been observed following dissociation of ketene at 212 nm [13] and at 193 nm [14], although at 193 nm may constitute only a minor branching in the dissociation [15,16]. Cleavage of the C–H bond has also been observed upon ketene excitation near the shortest absorption band limit at 193 nm [17] accounting for $\sim 37\%$ of the quantum yield for ketene dissociation [18]. However, experimental evidence indicates that, despite being exothermal, the C–H bond is not directly dissociated on the CH_2CO $(\tilde{B}\,^1B_1)$ surface when excited at wavelengths between 200 and 217 nm [11].

* Corresponding author. E-mail: mmm@iqfr.csic.es

0301-0104/98/$19.00
PII: S0301-0104(98)00145-1

Aiming to gain more information about the photodissociation dynamics of the $\tilde{B}\,^1B_1$ surface, in this work we have explored the region near the threshold for excitation of this excited singlet state; ketene has been dissociated at frequencies in the longest end limit of the $\tilde{X}\,^1A_1 \rightarrow \tilde{B}\,^1B_1$ absorption band and the nascent rotational population distribution in the CO photofragment has been measured.

2. Experimental

The experimental system was similar to that described in Ref. [19]. Samples of pure ketene at stagnation pressure $\sim$ 300 mbar, were expanded into a vacuum chamber through a pulsed piezoelectric valve (Laser Technics, 0.3 nm nozzle diameter). The frequency doubled output of a XeCl excimer pumped dye laser (Lambda Physik EMG 201/FL2002) was focused, $\sim$ 2 cm below the nozzle, by a 15 cm focal length lens. The frequency-doubled laser output was linearly polarized and provided $\sim$ 250 μJ per pulse at wavelength near 230 nm, with bandwidth of $\sim$ 0.3 cm^{-1} measured at the fundamental frequency. The same laser photolyzed the parent molecule and probed the photofragment CO, produced in the photodissociation. The CO rovibrational distribution was probed by a 2 + 1 REMPI scheme [20], scanning the laser wavelength over the two-photon resonance $CO(X\,^1\Sigma^+ \rightarrow B\,^1\Sigma^+)$. The photoions were accelerated by a set of parallel plates before entering a time-of-flight mass spectrometer provided with a pair of 1″ microchannel plates. The signal, after passing by a fast amplifier, was fed into a boxcar integrator (SRS250) interfaced to a personal computer for data storage and analysis.

Rough estimations of the rotational and vibrational temperatures in the jet were made using results obtained from previously recorded REMPI spectra of molecular beams of CO or CS_2, under several expansion conditions; the rovibrational population distributions measured from the REMPI spectra were used to estimate the temperatures in the parent molecular beam. For conditions similar to those of the present experiment, the estimated values were 50–60 K for the rotational temperature and around 200 K for the vibrational temperature.

3. Results and discussion

3.1. REMPI spectrum

REMPI spectra of the CO photofragment, formed by ketene photolysis, were recorded scanning the laser in steps of 0.0014 nm in the region from 229.92 to 230.55 nm. In this wavelength region the linearly polarized laser output, probes the rovibrational populations of $CO(X\,^1\Sigma^+)$ via the two-photon resonant transitions $X\,^1\Sigma^+ \rightarrow B\,^1\Sigma^+$. Each point was the average of 30 laser shots. The laser output was constant in energy over the whole scan with typical shot-to-shot laser energy fluctuations smaller than 3%. Parent molecule ions, which are most likely formed by 1 + 1 REMPI, were also monitored. Ketene photoions gave a constant signal over the whole range of scanned wavelengths, showing no spectral structure.

In Fig. 1a, the REMPI spectrum of the CO photofragment is shown. The *Q*-branches of the vibrational transitions $v'' = 0 \rightarrow v' = 0$ and $v'' = 1 \rightarrow v' = 1$ are observed. Lines starting in rotational levels up to $J'' = 50$ in $v'' = 0$ and up to $J'' = 37$ in $v'' = 1$ can be assigned.

3.2. Spectral simulation

The rotational population distribution of the $CO(X\,^1\Sigma^+)$ photofragment was obtained by simulation of the REMPI spectrum, using an analysis procedure based on a TSVD (truncated singular value decomposition) method, developed by Ruiz et al. [21] modified to deal with REMPI data. Ketene absorption probabilities were assumed to be constant in the small region of the REMPI scan (from 229.92 to 230.02) [12,22]. The experimental ionization intensities of the REMPI spectrum were assumed to be entirely determined by the $X\,^1\Sigma^+ \rightarrow B\,^1\Sigma^+$ two-photon transition probabilities [20].

Wavenumbers of the *Q*-branch lines of the $v'' = 0 \rightarrow v' = 0$ band were calculated from highly accurate molecular constants of the electronic states involved in the two-photon transition. For $CO(X\,^1\Sigma^+)$, we used the very consistent set of Dunham coefficients, calculated from a fit which includes energy levels up to $v = 41$ and $J = 93$ [23]. Term values for the upper state $B\,^1\Sigma^+$ were taken from Eidelsberg et al. [24].

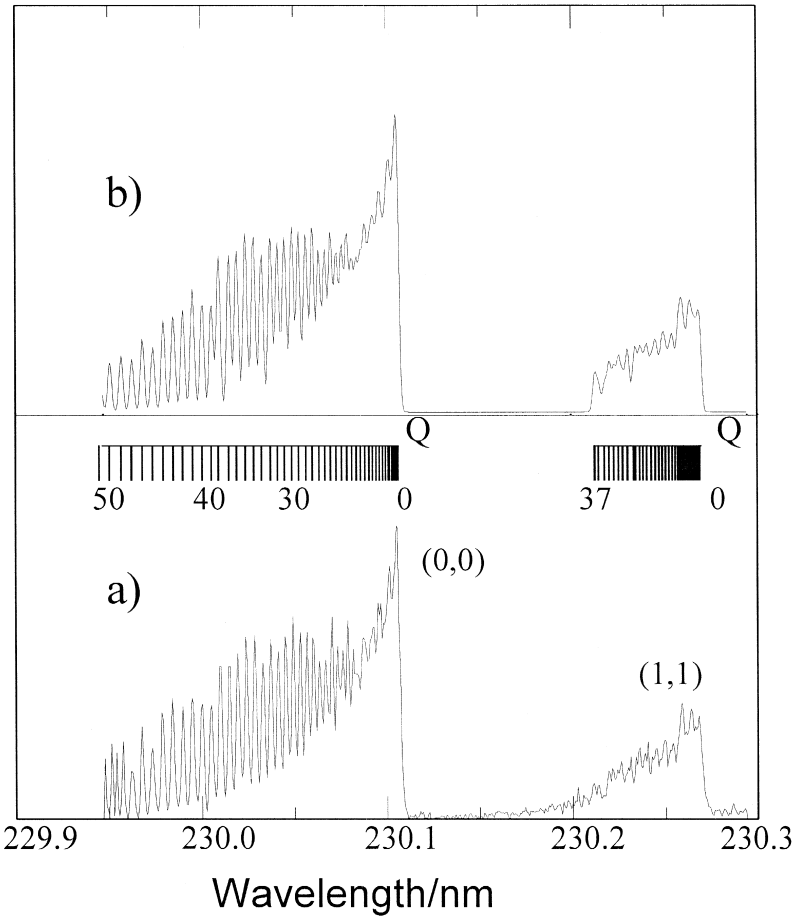

Fig. 1. (a) CO($B\,^1\Sigma^+ \leftarrow X\,^1\Sigma^+$) 2 + 1 REMPI spectrum, obtained in the laser photodissociation of ketene near 230 nm. (b) Spectrum calculated with the rotational distribution shown in Fig. 2.

For $B\,^1\Sigma^+$, $v' = 1$, accurate term values are only available up to $J' = 37$; therefore the spectral simulation of the $v'' = 1 \rightarrow v' = 1$ band was truncated at $J = 37$.

Potential energy curves for the two electronic states, needed to calculate wavefunctions and overlap integrals, were obtained in the following way. For the ground state $X\,^1\Sigma^+$, a RKR-V calculation was performed with extrapolation to the short- and long-range distances carried out by standard techniques [21]; the dissociation energy was taken from Eidelsberg et al. [24]. The upper state of the two-photon transition is a double-well potential due to an avoided crossing between the $D'\,^1\Sigma^+$ valence state and the $B\,^1\Sigma^+$ Rydberg state, converging to the same dissociation limit than the ground state. The potential energy curve obtained by Tchang-Brillet [25], based on a two-state diabatic model, extrapolated to short and long distances, was used in the present calculations. In this case the numerical procedure to generate the wavefunctions begun the inward integration at the maximum of the potential barrier, in a similar way as for quasibound states.

Finally, transition probabilities were calculated using the electronic transition moment function given by Tchang-Brillet [25]. The *Q*-branch rotational line strengths of two-photon transitions, for excitation with two identical linearly polarized photons, were taken from Halpern et al. [26]. The contribution from the allowed *O*- and *S*-branch two-photon transitions

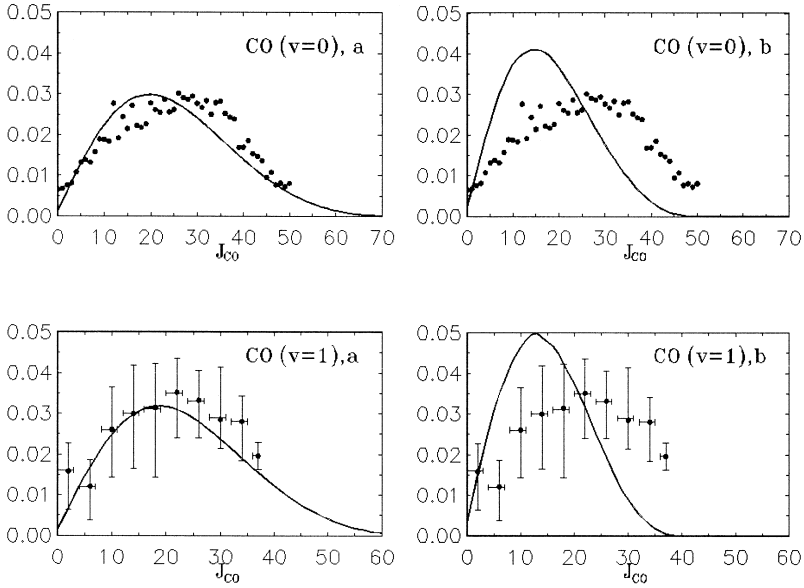

Fig. 2. Circles: CO($X\,^1\Sigma^+$, $v = 0$ and 1) rotational population distributions obtained from the experimental CO($B\,^1\Sigma^+ \leftarrow X\,^1\Sigma^+$) 2 + 1 REMPI spectrum, shown in Fig. 1. In $v = 1$ each point is the averaged populations of the four nearest rotational levels and the error bars indicate the minimum and maximum values. Full lines are the population distributions calculated by PST, for dissociation channels leading to $CH_2(\tilde{a}\,^1A_1)$ (a) and $CH_2(\tilde{b}\,^1B_1)$ (b), respectively.

is negligible, compared to the *Q*-branch [20], and were not included in the spectral simulation calculations.

The CO($X\,^1\Sigma^+$, $v = 0$ and 1) rotational distributions obtained by spectral simulation are given in Fig. 2a. The simulated spectrum can be compared to the experimental in Fig. 1b.

3.3. PST calculations

Some insight into the dynamics, governing the energy disposal to the products, can be obtained by comparing the photofragment experimental population distributions with that expected from statistical theories. Deviations from the direct statistical PST result, can reveal mode coupling and anharmonicity effects in barrierless reactions [27].

The completely statistical limit formulated in PST (phase space theory), has been applied recently to the dissociation of ketene, excited at different frequencies, on the first singlet potential surface $\tilde{A}\,^1A''(^1A_2)$ [1]. Rotational and vibrational distributions in $CH_2(\tilde{a}\,^1A_1)$ and CO have been compared to PST predictions, obtaining different degrees of agreement at the different dissociation energies. It has been found that PST predicts successfully rotational state distributions at subvibrational excitation of the products but underestimates product vibrational excitation at higher energies [1]. Marcus et al. [28,29] have explained this behavior on the assumption of the different motions of conserved and transitional modes after passing the transition state; following the latter assumption, they have compared the population distributions calculated by variational RRKM and PST for dissociation of ketene on the first excited singlet surface at several excess energies; they have found that RRKM and PST obtain similar rotational distributions, except when the excess energies are only slightly above the threshold for vibrational excitation of a particular conserved mode; in these cases, the RRKM-based treatment predicts a substantially increased vibrational excitation and large discrepancies in the rotational populations of the corresponding product vibrational state, are obtained [29].

In the present work, PST calculations have been applied to dissociation of ketene on the excited $\tilde{B}\,^1B_1$ surface, well above the threshold for formation of the $v = 0$ and 1 states of CO. We have calculated the

CO($v = 0$ and 1) rotational distributions predicted by PST for the dissociation channels leading to CO + $CH_2(\tilde{a}\,^1A_1)$ and to CO + $CH_2(\tilde{b}\,^1B_1)$, with excess energy of ~ 13500 and ~ 5200 cm^{-1}, respectively. To count the number of accessible states and calculate the final rotational distribution, we followed the steps given by Wade et al. [1]. The magnitudes needed for the calculation were evaluated as indicated below.

The excess energy available to the products, for each channel, was calculated from thermochemical and spectroscopic data.

The rotational level energies of ground-state ketene were calculated diagonalizing the Hamiltonian for the asymmetric top, using rotational and centrifugal distortion constants given by Johns et al. [30]. The initial rotational population distribution in the molecular beam of ketene was assumed to be Boltzmann, with rotational temperature of 60 K. The fraction of molecules in the ground vibrational level, calculated from a Boltzmann vibrational distribution at 200 K is ~ 0.9; values ranging from 0.01 to 0.03 are the fractional populations of molecules with one-quantum excitation in the low-frequency modes $\upsilon_9(b_2)$, $\upsilon_6(b_1)$ and $\upsilon_5(b_1)$; for simplicity, the calculation was restricted to the ground vibrational level.

For a given rotational state of ketene, the probability of photon absorption and dissociation was assumed to be governed only by the Hönl–London factors. Hönl–London factors for the perpendicular transition $^1A_1 \rightarrow {}^1B_1$ were taken from Herzberg [31].

Vibrational level energies of $CH_2(\tilde{a}\,^1A_1)$ were calculated within the harmonic oscillator approximation; the fundamental frequencies of the normal modes were taken from Jacox et al. [32]. Rotational level energies of $CH_2(\tilde{a}\,^1A_1)$ were calculated as those of the asymmetric top; *A*, *B* and *C* rotational constants were taken as a rough average of measured and calculated literature values for different rovibrational levels [32,33]. The calculated rovibrational level energies show a reasonably good degree of agreement with experimental determinations [33,34].

The slightly bent $CH_2(\tilde{b}\,^1B_1)$ was considered in the linear conformation; rovibrational level energies were calculated by the expressions of Herzberg et al. [35]. In the dissociation of ketene on the $\tilde{A}\,^1A_2(^1A'')$ surface, conservation of nuclear spin throughout dissociation has been experimentally tested [36]. Therefore, depending in each case on the total vibronic symmetry species, in the present calculations, rotational levels in CH_2CO and $CH_2(\tilde{a},\tilde{b})$ were treated separately according to their symmetry properties with respect to the permutation of the identical H nuclei. The final CO(υ) rotational PST distribution was obtained as the sum of each separated calculation weighted by their respective statistical factors.

The possibility of setting upper limits to the maximum orbital angular momentum, other than imposed by conservation laws, was also included in the calculations. This was done following Chen et al. [36], setting limits to the depth of a long-range potential well of the type $-C_6/r^6$ and to the range of impact parameters, b_{max}, between the separating fragments.

In Fig. 2, the PST CO($\upsilon = 0$ and 1) rotational population distributions can be compared to the experimental. The calculation corresponding to the dissociation channel leading to $CH_2(\tilde{a}\,^1A_1)$ matches the width of the experimental distribution, although it peaks at a rotational quantum number a few units smaller. On the other hand, the PST distribution calculated for the $CH_2(\tilde{B}\,^1B_1)$ exit channel is considerably narrower.

The calculated populations showed little dependence on the selection of the parameters C_6 and b_{max}, respectively in the ranges from 50000 cm^{-1} Å^{-6} and 3 Å, up to values corresponding to no restrictions to the orbital angular momentum.

The PST calculation for the dissociation pathway giving $CH_2(\tilde{B}\,^1B_2)$, leads to an average rotational energy in CO($\upsilon = 0$) of ~ 850 cm^{-1}, much smaller than the value of ~ 1550 cm^{-1} obtained from the experimental data; this suggests that this channel does not represent an important contribution to the dissociation process, and points towards the participation of a more exoergic pathway for the photofragmentation of the excited molecule. When formation of $CH_2(\tilde{a}\,^1A_1)$ is assumed, the calculated average rotational energy is ~ 1700 cm^{-1} which is much closer to the experimental value.

4. Final discussion

The lowest-lying singlet states of ketene are shown in Fig. 3 . The second excited singlet $\tilde{B}\,^1B_1$ is the only state that can be coupled to the ground state by

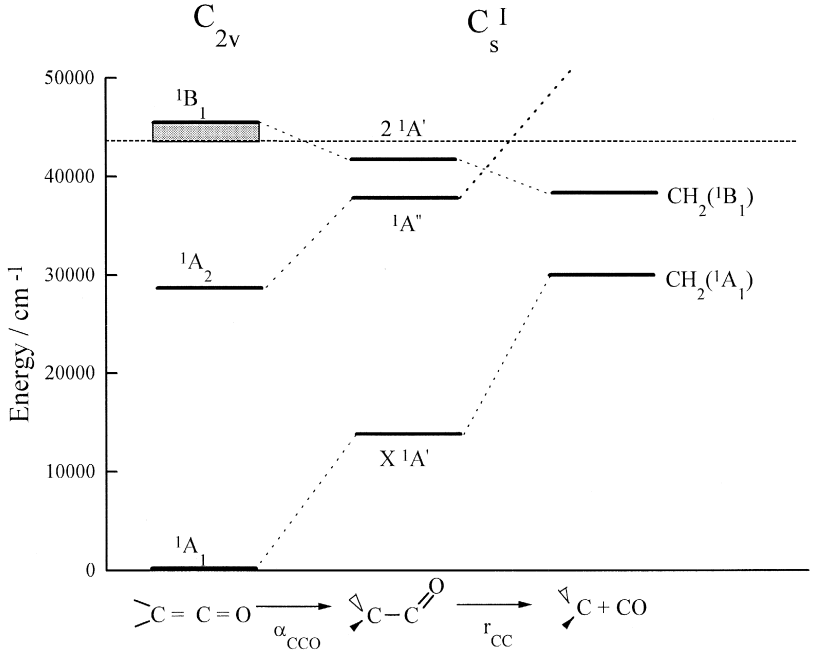

Fig. 3. State correlation diagram for dissociation of the lowest singlet states of ketene under the C_s-I (bent out-of-plane) symmetry. The energies of the $\tilde{X}\,^1A_1$, $\tilde{A}\,^1A_2$, $\tilde{B}\,^1B_1$ states in C_{2v} symmetry are vertical excitation energies [37,38]. For the $\tilde{B}\,^1B_1$ state, the shaded region indicates the energy region spanned by the absorption band [12,22] up to the energy corresponding to the vertical transition. The state energies of the parent molecule in the C_s-I symmetry are ab initio calculations for the optimized geometries at a C–C–O angle near 130° [37,38]. The dashed line corresponds to the energy of the absorbed photon at 230 nm.

an allowed optical transition by absorption at 230 nm. The transition can be described as the single-electron promotion $2b_1 \rightarrow 8a_1$, from an orbital having substantial π_{CC} bonding character to the lowest Rydberg 3s-like orbital [10,11,39,37]. Ketene is a slightly asymmetric top approaching a prolate symmetric top, with the near prolate top '*a*' axis along the CCO bond; for $\tilde{X}\,^1A_1 \rightarrow \tilde{B}\,^1B_1$ excitation, the only non-zero component of the transition dipole moment, M_x is perpendicular to the molecular plane; therefore molecules lying in a plane perpendicular to the laser field polarization vector will be preferentially excited. The same laser probes the CO($X\,^1\Sigma^+ \rightarrow \rightarrow B\,^1\Sigma^+$) two-photon transition. The two-photon transition moment consists of two perpendicular-type matrix elements, thus having a dominant Π non-resonant intermediate state, with some contribution from two parallel-type transition moments due to participation of Σ, also non-resonant, intermediate states [20,40]. In the dissociation of ketene, CO fragments remaining in-plane with respect to the molecular plane preferentially selected upon ketene absorption, will be more efficiently excited by the *X*-polarized probing laser.

Regarding the energetically available dissociation pathways of ketene excited in the $\tilde{B}\,^1B_1$ state, the most exoergic channel will be considered in the first place. The triplet $^3A_1$ state of ketene, lying ~ 37900 cm^{-1} above the ground state, has been observed by electron-impact energy-loss spectroscopy and assigned to a $\pi \rightarrow \pi*$ excitation in the CC double bond [41]; under the C_s-I geometry (CCO bent, CH_2 out-of-plane), the excited triplet, belongs to the symmetric species and correlates adiabatically to $CH_2(\tilde{X}\,^3B_1)$ and CO [38]; ab initio calculations of the potential energy surface along the dissociation coordinate indicate that direct intersystem crossing of this triplet with the two lowest singlet states in C_s-I, taking place at different energies, may influence the dissociation dynamics of the two lowest singlets [38]. The same calculations carried out at different CCO angles in the C_s-I geometry, obtain

that the $^3A_1(A')$ surface lies always at lower energies than the $\tilde{B}\,^1B_1(A')$ surface [37,38]; therefore no direct mechanism for the intersystem crossing occurs, suggesting that the pathway ending in triplet methylene cannot be an efficient dissociation channel.

Regarding the singlet channels, ab initio calculations show that the $\tilde{B}\,^1B_1$ state of ketene does not correlate with low-lying states of methylene under C_s-II symmetry (CCO bent, CH_2 in-plane). Dissociation along the C_{2v} geometry to $CH_2(\tilde{b}\,^1B_1)$ and CO is allowed [39]. However, it has been shown [37] that the $\tilde{B}\,^1B_1$ state stabilizes, breaking the C_{2v} symmetry upon bending of the CCO angle. The state correlation diagram shown in Fig. 3 summarizes recent theoretical results for the dissociation of the three lowest singlet states of ketene along the C_s-I geometry [10,37,38,42]. The energy of the $\tilde{B}\,^1B_1(2^1A')$ state is lowered upon bending of the CCO angle [37], decreases monotonically as the CC bond stretches and after crossing the $\tilde{A}\,^1A_2(^1A'')$ surface, correlates to the products $CH_2(\tilde{b}\,^1B_1)$ and CO. In this case, unlike dissociation from the first excited singlet of ketene, which crosses extensively the ground state around the Franck–Condon region in the C_s-II symmetry [10,38,42], surface crossing does not provide a direct pathway between the $\tilde{B}\,^1B_1$ and ground state. However, even in the absence of this direct pathway, weak electron–nuclear coupling can mix levels of similar energies in different electronic states, opening an indirect path to dissociation on a lower electronic surface; moreover, it has been pointed out that this mechanism would result in an energy disposal in the photo-products which may tend to be statistically rather than dynamically controlled [43].

The comparison between the experimental population distribution in CO and the PST calculation indicates that the statistical limit would be compatible with dissociation along a pathway that released larger excess energy than required for $CH_2(\tilde{b}\,^1B_1)$ formation; we tentatively conclude that the latter can only be a minor dissociation channel and therefore, ketene excited near the threshold for formation of the $\tilde{B}\,^1B_1$ state, probably undergoes internal conversion and dissociates along the ground singlet surface.

Finally, we note that for dissociation of ketene along the first excited singlet, it has been observed [1] that the dynamics of CO are close to the statistical limit but somewhat constrained to populate a narrower range of quantum states, while the dynamics for singlet methylene are far from statistical and considerably colder than predicted by the PST limit [5]. It seems an obvious conclusion that a further characterization of the dissociation process would require some knowledge about the state distributions of the methylene fragment. Work to obtain some information about the population distribution in $CH_2(\tilde{a}\,^1A_1)$ is in progress.

Acknowledgements

Financial support has been provided by the Ultraviolet Laser Facility operating at FORTH–IESL under the Large Installations Plan of EEC; special thanks are given to M. Tzatzadaki for technical assistance. The authors are grateful to Dr. Lydia Tchang-Brillet for providing the $CO(B\,^1\Sigma^+)$ potential energy curve and $CO(B\,^1\Sigma^+ \leftarrow X\,^1\Sigma^+)$ transition dipole moment and to Dr. R. Escribano for the computer program to calculate rovibrational energy levels of an asymmetric top. This work has been supported in part by Spanish DGICYT (PB96-0844-CO2-01).

References

[1] E.A. Wade, H. Clauberg, S.K. Kim, A. Mellinger, C.B. Moore, J. Phys. Chem. A 101 (1997) 732.
[2] W.H. Green Jr., I.-C. Chen, C.B. Moore, Ber. Bunsenges. Phys. Chem. 92 (1988) 389.
[3] I.-C. Chen, C.B. Moore, J. Phys. Chem. 94 (1990) 263.
[4] I. Garcia-Moreno, E.R. Lovejoy, C.B. Moore, J. Chem. Phys. 100 (1994) 8890.
[5] I. García-Moreno, E.R. Lovejoy, C.B. Moore, J. Chem. Phys. 100 (1994) 8902.
[6] S.J. Klippenstein, A.L.L. East, W.D. Allen, J. Chem. Phys. 101 (1994) 9198.
[7] E.D. Potter, M. Gruebele, L.R. Khundkar, A.H. Zewail, Chem. Phys. Lett. 164 (1989) 463.
[8] S.K. Kim, Y.S. Choi, C.D. Pibel, Q.-K. Zheng, C.B. Moore, J. Chem. Phys. 94 (1991) 1954.
[9] C.G. Morgan, M. Drabbels, A.M. Wodtke, J. Chem. Phys. 104 (1996) 7460.
[10] W.D. Allen, H.F. Schaefer III, J. Chem. Phys. 84 (1986) 2212.
[11] X. Liu, S.G. Westre, J.D. Getty, P.B. Kelly, Chem. Phys. Lett. 188 (1992) 42.
[12] J.W. Rabalais, J.M. McDonald, V. Scherr, S.P. McGlynn, Chem. Rev. 71 (1971) 73.

[13] M. Castillejo, M. Martin, R. de Nalda, M. Oujja, Chem. Phys. Lett. 237 (1995) 367.
[14] J. Ruiz, M. Martin, Chem. Phys. Lett. 226 (1994) 300.
[15] B.I. Sonobe, R.N. Rosenfeld, J. Am. Chem. Soc. 105 (1983) 7528.
[16] G.T. Fujimoto, M.E. Umstead, M.C. Lin, Chem. Phys. Lett. 65 (1982) 197.
[17] K.G. Unfried, G.P. Glass, R.F. Curl, Chem. Phys. Lett. 177 (1991) 33.
[18] L.R. Brock, B. Mischler, E. Rohlfing, R.T. Bise, D.M. Neumark, J. Chem. Phys. 107 (1997) 665.
[19] S. Couris, E. Patsilinakou, M. Lotz, E.R. Grant, C. Fotakis, C. Cossart-Magos, M. Horani, J. Chem. Phys. 100 (1994) 3514.
[20] P.J.H. Tjossem, K.C. Smyth, J. Chem. Phys. 91 (1989) 2041.
[21] J. Ruiz, M. Martin, Comput. Chem. 19 (1995) 417.
[22] W.C. Price, J.P. Teegan, A.D. Walsh, J. Chem. Soc. London Part I (1951) 920.
[23] G. Guelachvili, D. de Villeneuve, R. Farrenq, W. Urban, J. Veges, J. Mol. Spectrosc. 98 (1983) 64.
[24] M. Eidelsberg, J.-Y. Roncin, A. Le Floch, F. Launay, C. Letzelter, J. Rostas, J. Mol. Spectrosc. 121 (1987) 309.
[25] W.-ÜL Tchang-Brillet, P.S. Julienne, J.-M. Robbe, C. Letzelter, F. Rostas, J. Chem. Phys. 96 (1992) 6735.
[26] J.B. Halpern, H. Zacharias, R. Wallenstein, J. Mol. Spectrosc. 79 (1980) 1.
[27] S.J. Klippenstein, A.L.L. East, W.D. Allen, J. Chem. Phys. 105 (1996) 118.
[28] R.A. Marcus, Chem. Phys. Lett. 144 (1988) 208.
[29] S.J. Klippenstein, R.A. Marcus, J. Chem. Phys. 91 (1989) 2280.
[30] J.W.C. Johns, L. Nemes, K.M.T. Yamada, T.Y. Wang, J.L. Domenech, J. Santos, P. Cancio, D. Bermejo, J. Ortigoso, R. Escribano, J. Mol. Spectrosc. 156 (1992) 501.
[31] G. Herzberg, Molecular Spectra and Molecular Structure, III. Electronic Spectra and Electronic Structure of Polyatomic Molecules, Van Nostrand Reinhold, New York, 1965, p.232.
[32] M. Jacox, J. Phys. Chem. Ref. Data 17 (1988) 269.
[33] W.H. Green Jr., N.C. Handy, P.J. Knowles, S. Carter, J. Chem. Phys. 94 (1991) 118.
[34] A. Alijah, G. Duxbury, Mol. Phys. 70 (1990) 605.
[35] G. Herzberg, J.W.C. Johns, Proc. R. Soc. London, Ser. A 295 (1966) 107.
[36] I.-C. Chen, W.H. Green Jr., C.B. Moore, J. Chem. Phys. 89 (1988) 314.
[37] P.G. Szalay, A.G. Császár, L. Nemes, J. Chem. Phys. 105 (1996) 1034.
[38] Q. Cui, K. Morokuma, J. Chem. Phys. 107 (1997) 4951.
[39] W.D. Allen, H.F. Schaefer III, J. Chem. Phys. 89 (1988) 329.
[40] K.M. Beck, K.A.H. German, W.P. Hess, Chem. Phys. Lett. 256 (1996) 297.
[41] R.P. Fruelholz, W.M. Flicker, A. Kuppermann, Chem. Phys. Lett. 38 (1976) 57.
[42] S. Yamabe, K. Morokuma, J. Am. Chem. Soc. 100 (1978) 7551.
[43] R.N. Dixon, Chem. Soc. Rev. (1994) 375.